Electronic Supplementary Material (ESI) for Dalton Transactions.
This journal is © The Royal Society of Chemistry 2023

Electronic Supplementary Information

The Rigidity and Chelation Effect of Ligands on the Hydrogen Evolution Reaction Catalyzed by Ni(II) Complexes

Anjali Mishra,[a] Gaurav Kumar Mishra,[b] Anamika,[a] Nanhai Singh,[a] Rama Kant,*[b] and Kamlesh Kumar*[a]

[a]Department of Chemistry, Institute of Science, Banaras Hindu University, Varanasi 221005, India, E-mail: kamlesh.kumar@bhu.ac.in,

[b]Department of Chemistry, University of Delhi, Delhi-110007, India, Email: rkant@chemistry.du.ac.in

Contents in Supporting Information

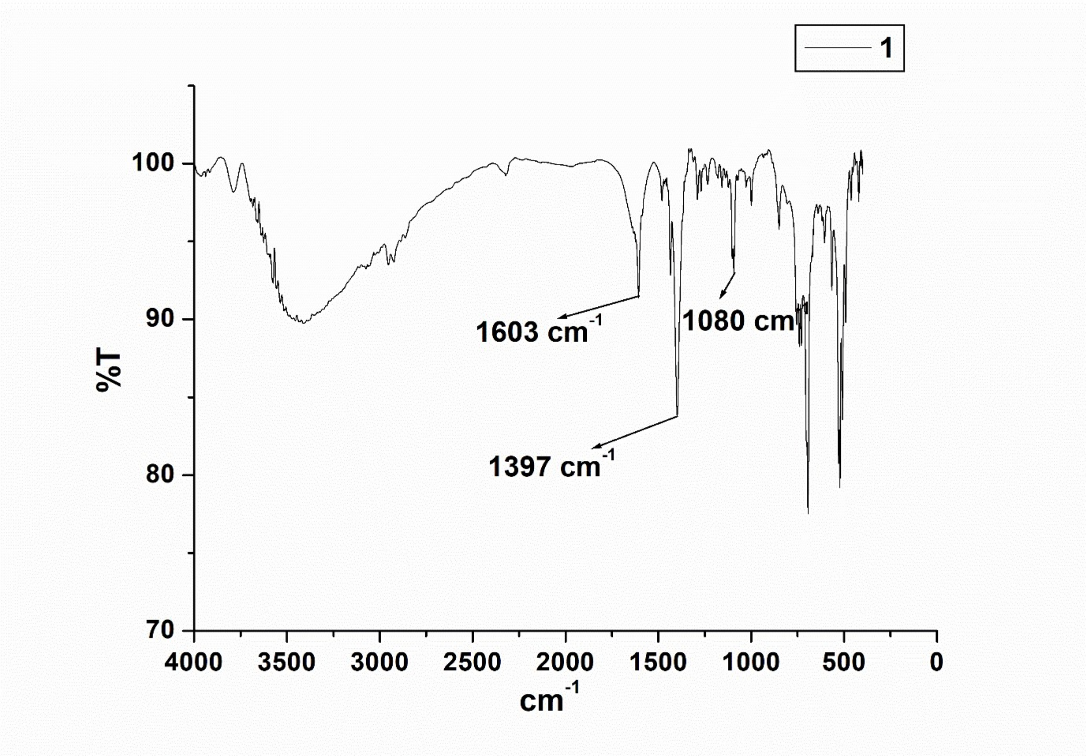

Figure S1. FT-IR spectrum of Complex **1.**

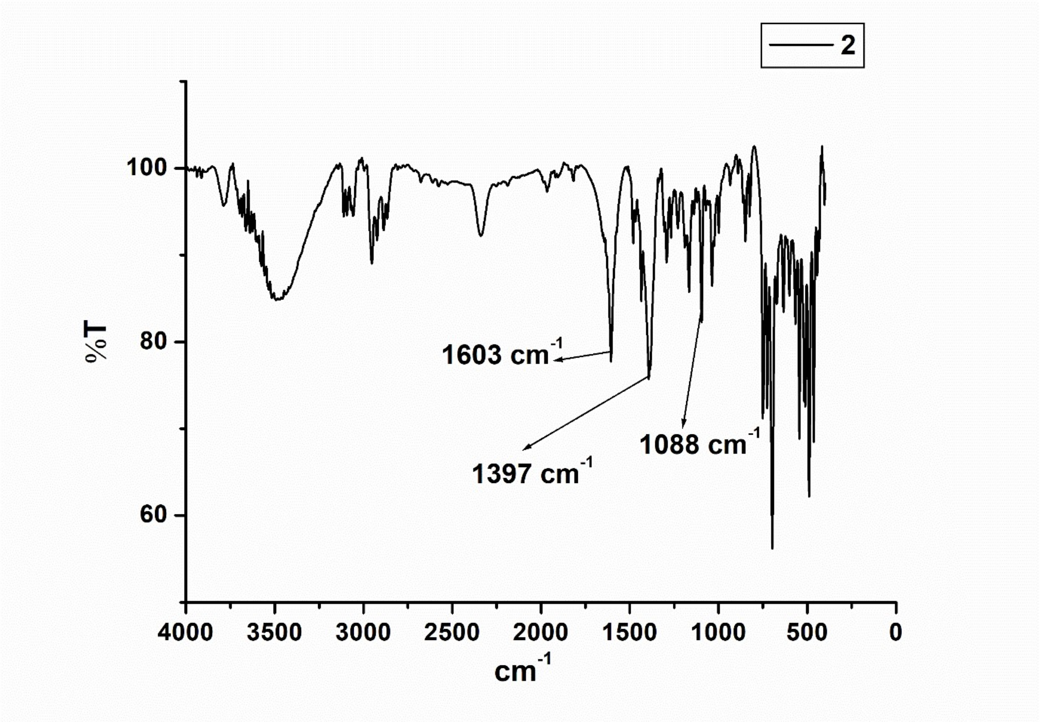

Figure S2. FT-IR spectrum of Complex **2**.

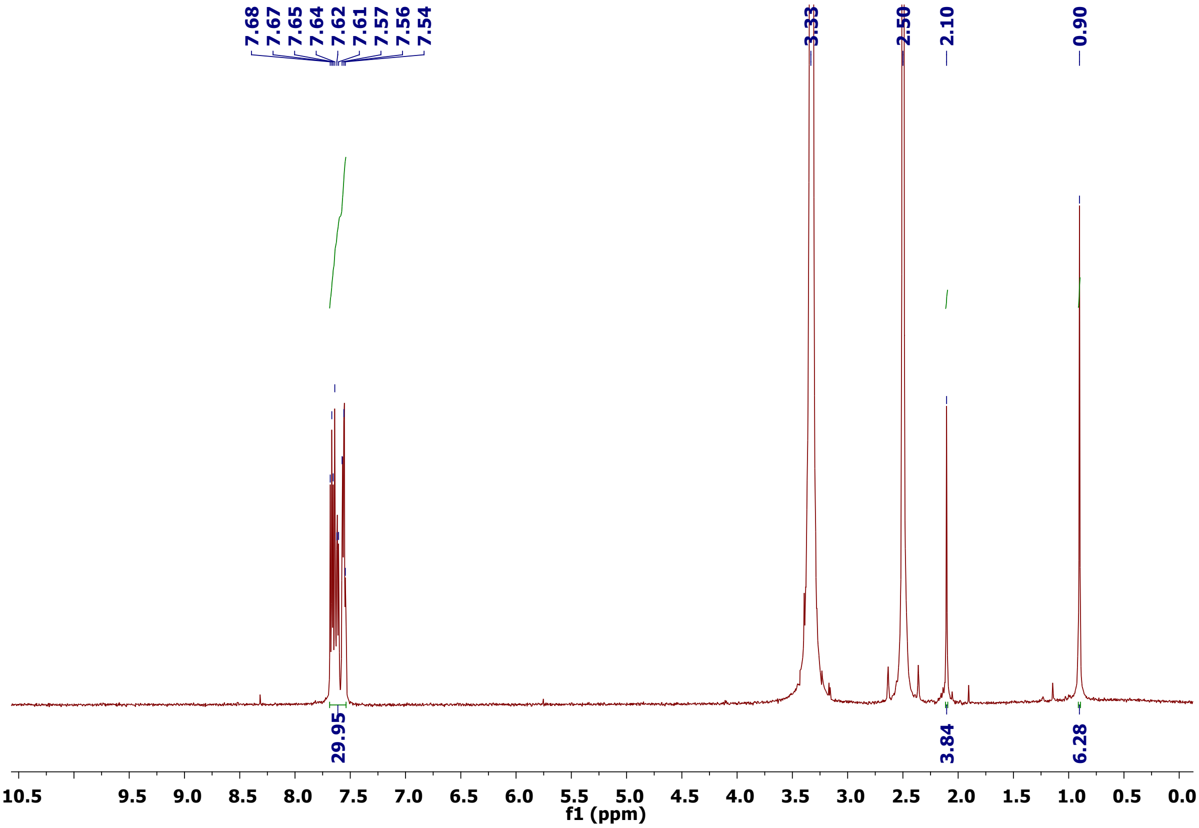

Figure S3. ^{1}H NMR spectrum of complex **1** (500 MHz, $(CD_3)_2SO$).

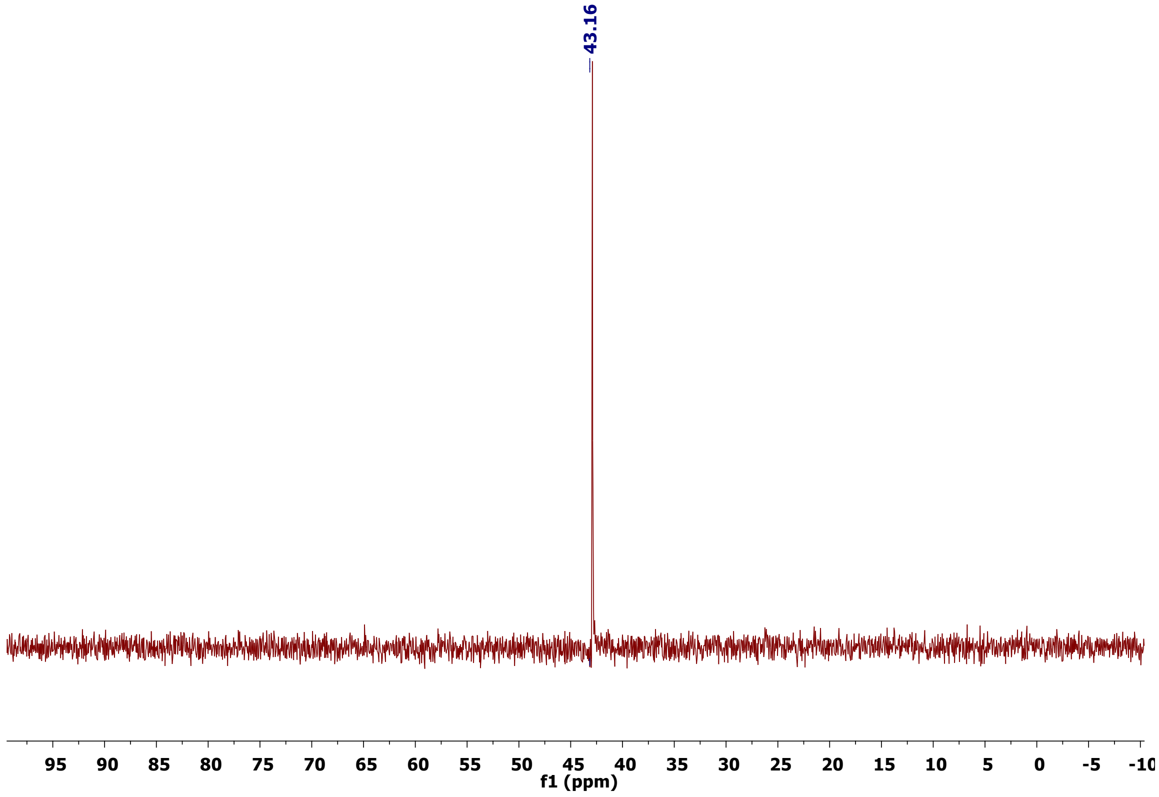

Figure S4. $^{31}P\{^{1}H\}$ NMR Spectrum of complex **1** (202 MHz, $(CD_3)_2SO$)

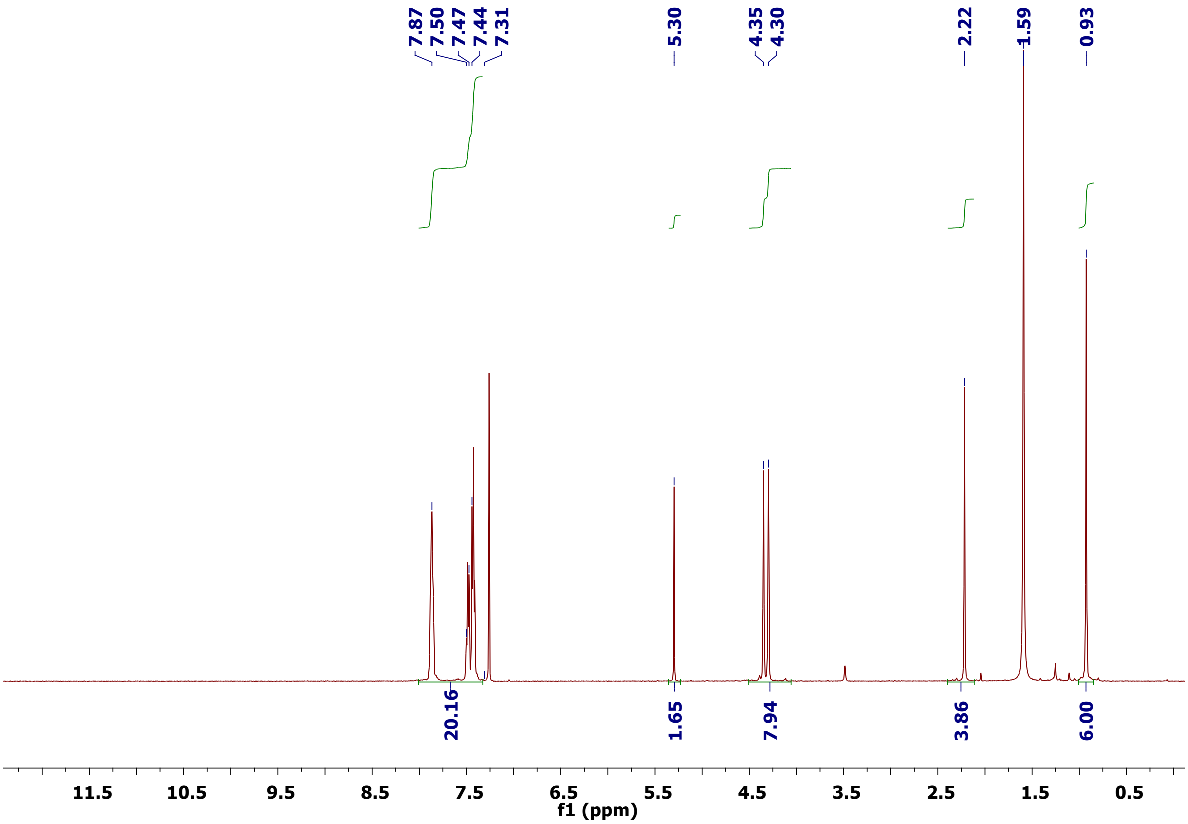

Figure S5. ^{1}H NMR spectrum of complex **2** (500 MHz, $CDCl_3$).

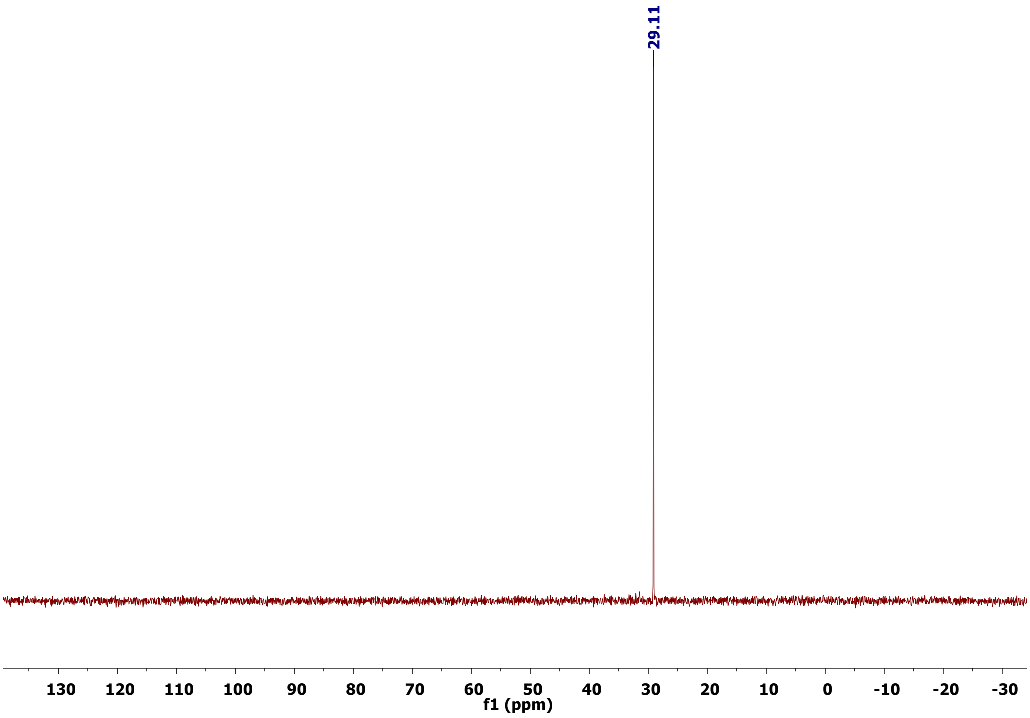

Figure S6. $^{31}P\{^{1}H\}$ NMR spectrum of complex **2** (202 MHz, $CDCl_3$)**.**

Table S1. Crystal data and structure refinement for complex 2

Complex	**2**. CH_2Cl_2
Empirical Formula	$C_{44}H_{40}FeNiO_2P_2S_2Cl_2$
Formula weight	912.28
Temperature/K	100
Crystal System	monoclinic
Space group	$P2_1/n$
a/Å	11.2514(8)
b/Å	15.9569(12)
c/Å	22.9243(18)
α/°	90
β/°	103.348(2)
γ/°	90
Volume/Å^3	4004.6(5)
Z	4
ρ_{calc}g/cm^3	1.513
μ/mm^{-1}	1.888
F(000)	1880.0
Radiation	MoKα (λ = 0.71073)
2Θ range for data collection/°	4.456 to 56.66
Index ranges	$-15 \leq h \leq 15$, $-21 \leq k \leq 21$, $-30 \leq 1 \leq 30$
Reflections collected	59123
Independent reflections	9957 [R_{int} = 0.0451, R_{sigma}= 0.0306
Data/restraints/parameters	9957/0/489
Goodness-of-fit on F^2	1.115
Final R indexes [I>=2σ (I)]	R_1 = 0.0357, wR_2 = 0.0652
Final R indexes [all data]	R_1 = 0.0444, wR_2 = 0.0696
Largest diff. peak/hole / e Å^{-3}	0.72/-0.72
CCDC No.	2259175

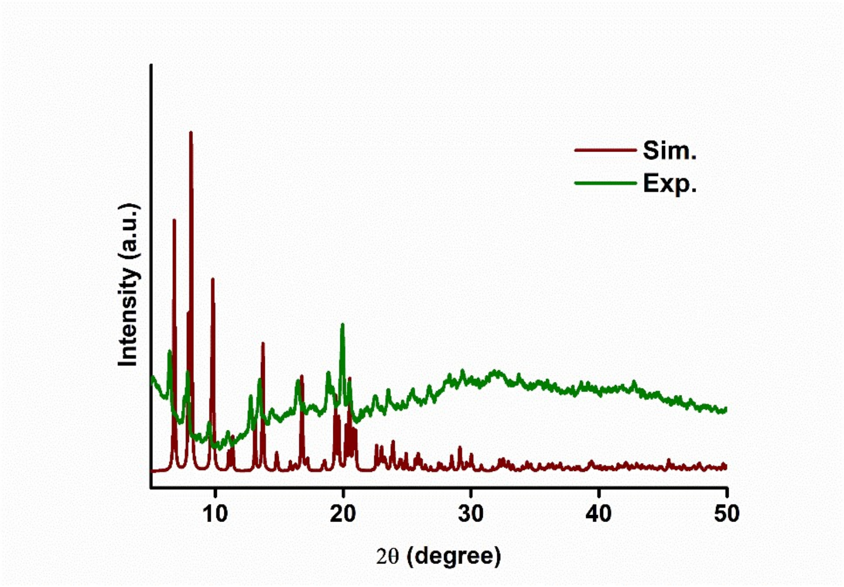

Figure S7. Simulated and experimental PXRD patterns of complex **2**.

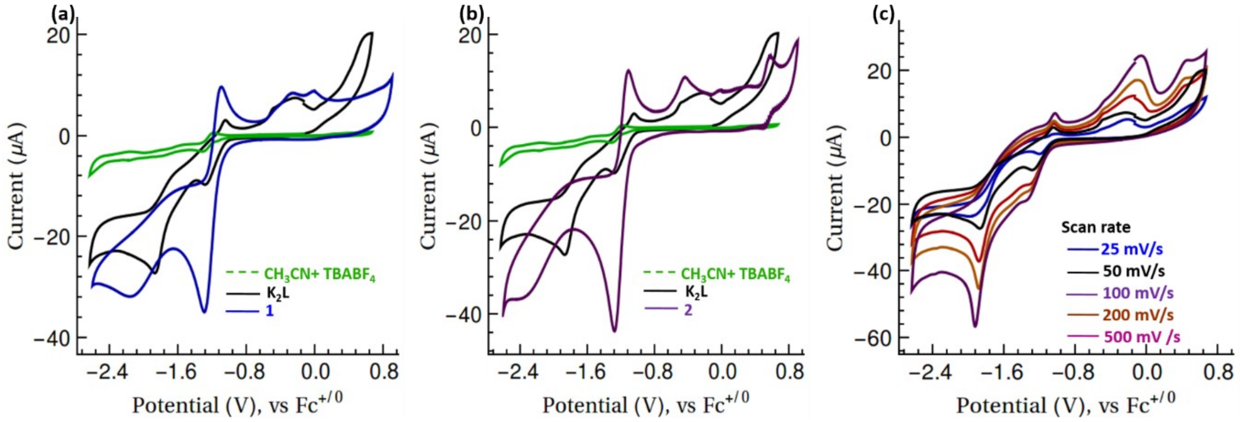

Figure S8. (a) Comparison of CVs of blank (CH_3CN + 0.1 M $TBABF_4$ as green), 2 mM of **K_2L** ligand (black),1mM of **1** (blue), and (b) **2** (purple) in CH_3CN containing 0.1 M $TBABF_4$ at 100 mV/s, (c) effect of scan rate variation on the peak currents of (**K_2L**).

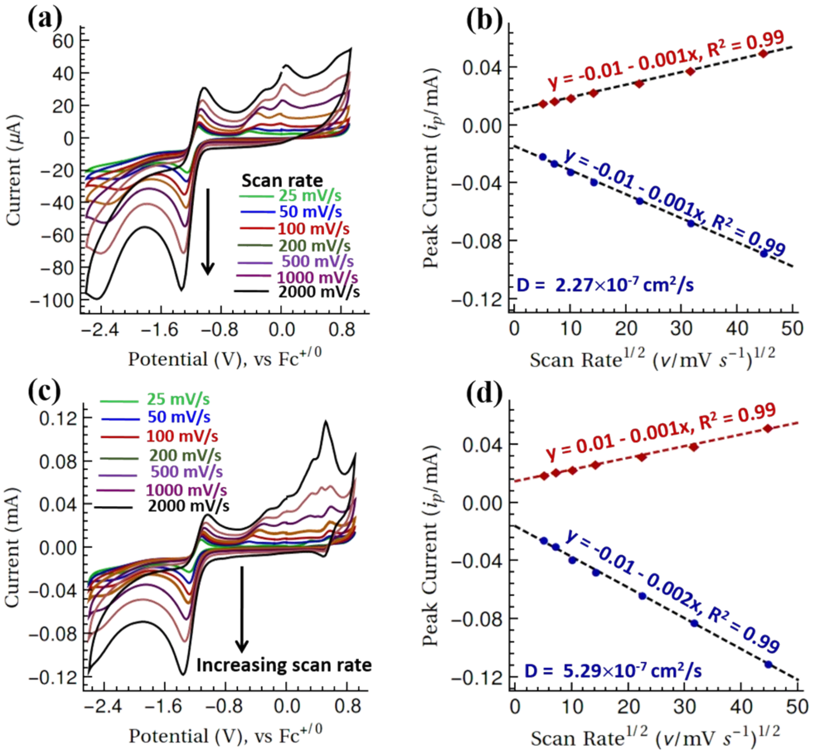

Figure S9. (a) Effect of variation of scan rate from 25 mV/s to 2000 mV/s on cyclic voltammogram of 1 mM complex **1** (a) and **2** (c) in CH_3CN containing 0.1 M $TBABF_4$. Fig. (b) and (d) show the variation of peak current with the square root of scan rate for complexes **1** and **2**, respectively. The calculated value of diffusion coefficient from the slope (using eq 1, D (or D_{cat}) is listed.

Randles–Ševčík Equation.

The linear variation of peak currents with the square root of the scan rate represents the diffusion-controlled phenomena. The slope of the best-fit equation (Randles-Sevcik equation) provides the diffusion coefficient of the catalyst using

$$i_p = 0.4463nFA[C]\left(\frac{nF\nu D_{cat}}{RT}\right)^{1/2} \text{..........} \qquad \text{(S1)}$$

where, I_p = peak current, n = 1 (number of electron transferred),

A = 0.0214 cm^2 (Electrode area), F = 96500 C/mole (Faraday constant),

R = 8.314 J/K/mole (Gas constant), T = 298 K (Temperature),

D_{cat} = diffusion coefficient of catalyst, ν = Scan rate (V/s)

Overpotential Calculations.

For overpotential estimation, $E^{T}_{1/2}$ (= E_{ref}) is calculated using $E^{0}_{H^{+}/H_2}$, pKa, ε_D and $C^{0}_{H_2}$ by applying the Fourmond's approach[1], given by

$$E^{T}_{1/2} = E^{0}_{H^{+}/H_2} - \mathbf{2.303}\,\frac{RT}{F}\,\mathbf{pK_a} + \boldsymbol{\varepsilon}_{\mathbf{D}} - \frac{RT}{2F}\ln\frac{c_0}{C^{0}_{H_2}}\ldots\ldots \qquad \text{(S2)}$$

$E^{T}_{1/2}$ in 15 mM CF_3COOH in CH_3CN is estimated as,

$$E^{T}_{1/2} = (-0.07) - 2.303\,\frac{8.314 \times 298}{96485}\,12.7 + 0.040 - \frac{8.314 \times 298}{2 \times 96485}\ln\frac{15}{3.3}$$

$$E^{T}_{1/2} = -0.80 \text{ V versus } Fc^{+/0}$$

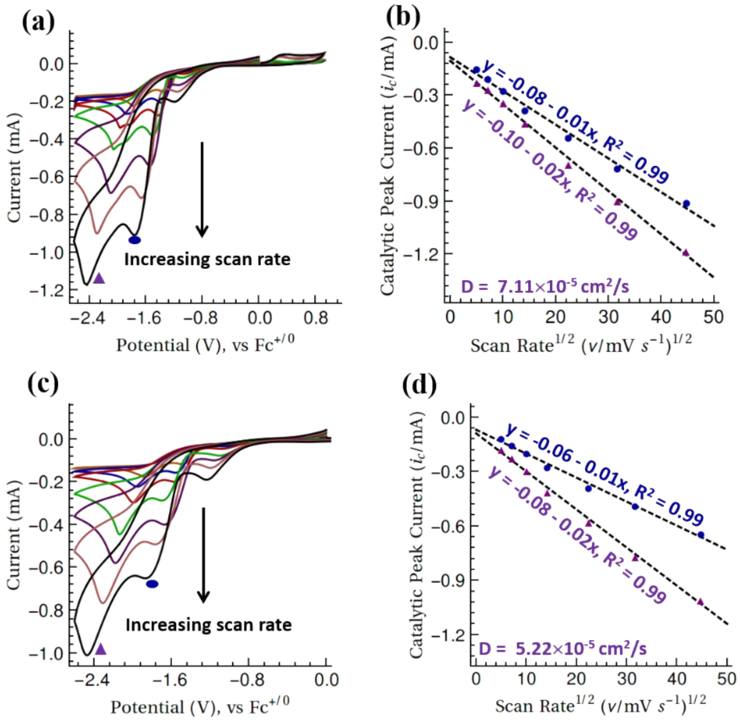

Figure S10. (a) Variation of scan rate from 25 mV/s to 2000 mV/s of 1 mM complex **1** (a) and **2** (c) in the presence of 15 mM TFA in CH_3CN containing 0.1 M $TBABF_4$, Plot (b) and (d) show the variation of catalytic peak current with the square root of scan rate for complex **1** and **2,** respectively.

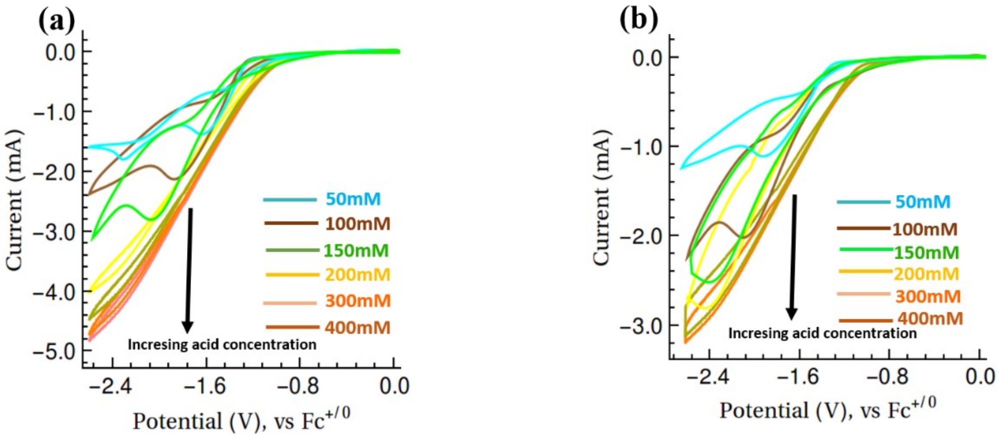

Figure S11. CV of 1 mM complex **1** (a) and **2** (b) on varying acid (TFA) concentration in CH_3CN, containing 0.1 M $TBABF_4$ at scan rate 200 mV/s.

Foot-of-the-wave analysis (FOWA): Determination of rate-determining step for ECEC mechanism

For the ECEC mechanism with the multi-electron and proton transfer process, the expression of the current is given by equation[2]:

$$i = \frac{i_{cat}}{1 + e^{\left[\frac{RT}{F}(E - E_{cat/2})\right]}} \text{ .... (S3)}$$

where,

$$i_{cat=} \; 2FS[Cat]\sqrt{D_{cat}}\frac{1}{\frac{1}{\sqrt{k_1 + [H^+]}} + \frac{1}{\sqrt{k_2[H^+]}}} \text{ .... (S4)}$$

Here i_{cat} represents the catalytic plateau current, T is the temperature, F is the Faraday constant, R is the gas constant, $E_{cat/2}$ is the catalytic half-wave potential, A is the surface of the electrode, D_{cat} the diffusion coefficient of catalyst, [Cat] is the concentration of the catalyst, $[H^+]$ is the concentration of acid. The first and second protonation rate constants are defined by k_1 and k_2, respectively.

Dividing eq. S3 by the peak current (i_p) for the reversible one-electron transfer (Randles-Ševčík equation in eq S1), simplifies eq. S3 as,

$$\frac{i}{i_p} = \frac{i_{cat}}{i_p} \times \frac{1}{1 + e^{\left[\frac{F}{RT}\left(E - E_{cat/2}\right)\right]}} \quad \text{..................(S5)}$$

Plotting the catalytic enhancement (i/i_p) as a function of the foot of wave axis $\frac{1}{1 + e^{\left[\frac{F}{RT}\left(E - E_{cat/2}\right)\right]}}$, gives a linear curve near the foot of the catalytic wave. The slope provides the estimation of relevant rate constants. The two important classifications for the protonation step are:

(i) $k_2 >> k_1$, i.e., the rate-determining step is the first protonation step,

(ii) $k_1 >> k_2$, i.e., the rate-determining step is the second protonation step.

The $E_{cat/2}$ relation with the formal potential of the $Ni^{II/I}$ redox couple (E^0) that triggers the catalytic process is given by[2]

$$E_{cat/2} = E^0 + \frac{RT}{F} ln\left(\frac{k_1}{k_2}\right) \quad \text{......................(S6)}$$

Equation S6 signifies that $E_{cat/2}$ is more negative than E^0 leading to $k_1<k_2$ and vice-versa. Figure S12 (a) and (b) for complexes **1** and **2** show the linear variation of current with the FOW-axis and indicate that $E_{cat/2}$ is more negative than E^0 confirming that the first protonation step resulting in the formation of Ni^{III}-H is the rate-determining step.

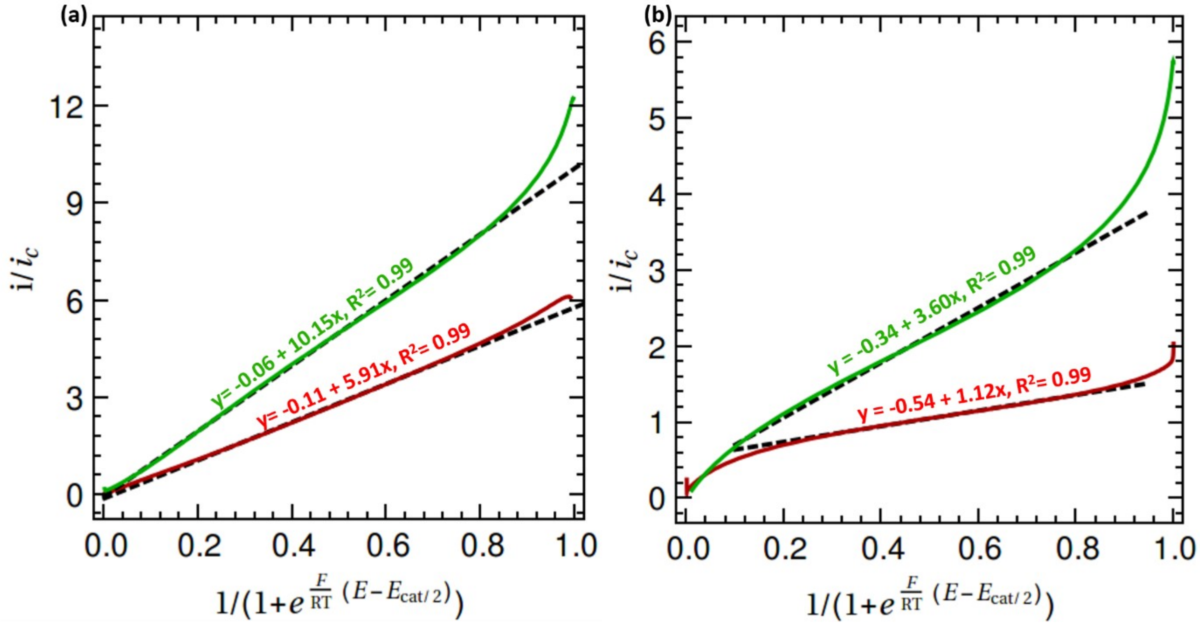

Figure S12. Plot of i/i_p versus foot of wave axis for ECEC mechanisms for complex **1** in plot (a) and **2** in the plot (b) is generated for 10 mM (red curve) and 15 mM (green curve) of TFA for 1 mM of **1** and **2** in CH_3CN containing 0.1 M $TBABF_4$ at 200 mV/s**.** The dashed black line is the best fit which shows the linear variation of current with the foot of the wave axis. This confirms that $k_1 << k_2$.

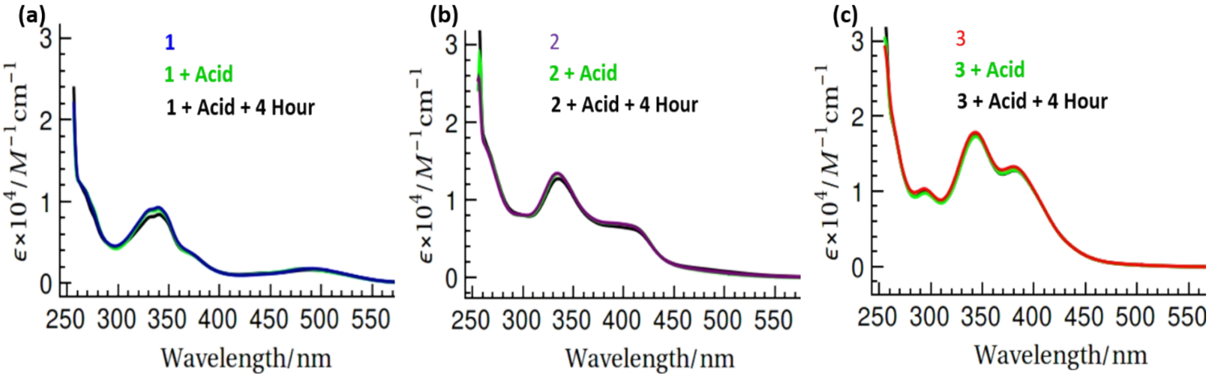

Figure S13. UV-Vis spectra of complexes **1–3** in acetonitrile solution at 10^{-4} molar concentration in the presence of 25 equivalents of trifluoro acetic acid.

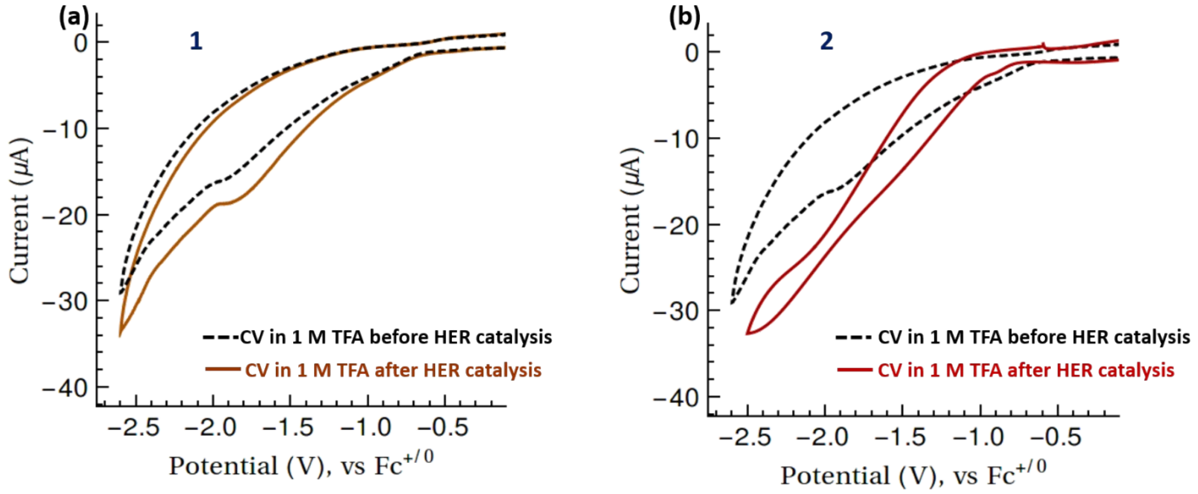

Figure S14. Dashed black line corresponds to 1M TFA solution before the catalytic experiment and the solid red line is after the catalysis experiment in 1M TFA solution at 200 mV/s scan rate. No appearance of a catalytic peak signifies that no nano-particulated substance or complex **1** and **2** is deposited on the glassy carbon electrode surface.

Table S2. Comparison of the recently synthesized Ni(II) chelate complexes to decipher the electronic and geometric effects in HER catalysis in the presence of TFA as a proton source.

S. No.	Complex Ni(LL')	Solvent	Overpotential (η) (mV)	TOF (s^{-1})	Reference
1.	$Ni[P_2S_2C_2(C_6H_4R\text{-}P)_2]$, R= CH_3O	DMF	1020	802	Zhang et al., 2023[3]
2.	$Ni[P_2S_2C_2(C_6H_4R\text{-}P)_2]$, R= CH_3	DMF	1000	894	Zhang et al., 2023[3]
3.	$Ni[P_2S_2C_2(C_6H_4R\text{-}P)_2]$, R= H	DMF	970	872	Zhang et al., 2023[3]
4.	$Ni[P_2S_2C_2(C_6H_4R\text{-}P)_2]$, R= Br	DMF	910	557	Zhang et al., 2023[3]
5.	$Ni[P_2S_2C_2(C_6H_4R\text{-}P)_2]$, R= F	DMF	950	423	Zhang et al., 2023[3]
6.	$(N_2S_2)Ni(II)$	$CH_3CN + H_2O$	730	1250	Mirica et al.[4], 2022

7.	Ni(dmbpy)(mp)	CH_3CN	720	47,160	Mitsopoulou et al.[5], 2021
8.	Ni(bpy)(mp)	CH_3CN	580	5544	Mitsopoulou et al.[5], 2021
9.	(Ar_4)PNi(II)	CH_3CN	~880*	-	Qiu et al.[6], 2023
10.	(F_5Ph)PNi(II)	CH_3CN	~800*	-	Qiu et al.[6], 2023
11.	Ni(L4)$^{+2}$	CH_3CN	1070	220	Lau et al.[7], 2015
12.	**1**	CH_3CN	450	3283	This work
13.	**2**	CH_3CN	640	1049	This work
14.	**3**	CH_3CN	1012	-	This work

* The $E_{1/2}$ value is calculated from CV (Fig 5 and S24) following this, overpotential is calculated at 15mM TFA.

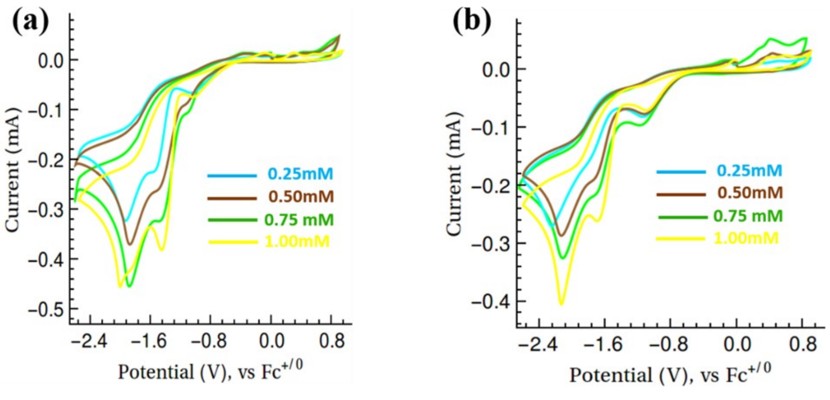

Figure S15. CV of complex **1** (a) and **2** (b) on varying concentrations of the complex in CH_3CN, containing 0.1 M $TBABF_4$ and 15 mM TFA at 200mV/s scan rate.

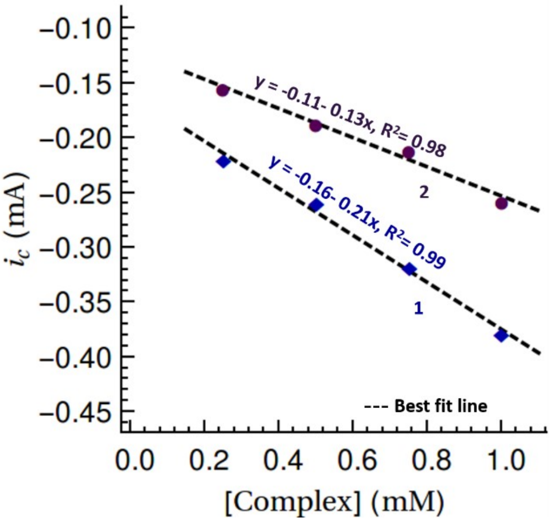

Figure S16. Plot of catalytic peak current i_c, versus varying concentrations of complex **1** (blue diamond) and **2** (purple circle) in CH_3CN containing 0.1 M $TBABF_4$ and 15 mM TFA at 200 mV/s.

References

1. V. Fourmond, P.-A. Jacques, M. Fontecave and V. Artero, *Inorg. Chem.*, 2010, **49**, 10338-10347.
2. V. C. C. Wang and B. A. Johnson, *ACS Catal.*, 2019, **9**, 7109-7123.
3. L. Chen, T. Li, B. Xie, C. Lai, R.-W. Ji, J.-Y. He, J.-X. Cao, M.-N. Liu, W. Li and D.-L. Zhang, *Catalysis Science & Technology*, 2023, **13**, 3655-3666.
4. S. Sinha, G. N. Tran, H. Na and L. M. Mirica, *Chem Commun (Camb)*, 2022, **58**, 1143-1146.
5. F. Kamatsos, K. Bethanis and C. A. Mitsopoulou, *Catalysts*, 2021, **11**, 401.
6. S. Xue, X. Lv, N. Liu, Q. Zhang, H. Lei, R. Cao and F. Qiu, *Inorg. Chem.*, 2023, **62**, 1679-1685.
7. L. Chen, G. Chen, C.-F. Leung, S.-M. Yiu, C.-C. Ko, E. Anxolabéhère-Mallart, M. Robert and T.-C. Lau, *ACS Catal.*, 2015, **5**, 356-364.